Basic Study on Effect of Repetitive Perfect Tracking Control on Iron Loss of IPMSM

Yuhiro Inagaki* Student Member, Masahiro Mae* Student Member
Osamu Shimizu* Member, Sakahisa Nagai* Member
Hiroshi Fujimoto* Senior Member, Takayuki Miyajima** Member
Yoshiki Yasuda** Member, Akio Yamagiwa** Member

Permanent magnet synchronous motor (PMSM) has wide range of usage opportunities due to its many advantages. In order to achieve efficient driving of PMSM, a number of high efficiency control methods have been developed. However, there are few researches that discuss the relationship between tracking characteristics to the current command and driving loss. In this paper, we propose to apply repetitive perfect tracking control (RPTC), which is the current control with high tracking performance to the current command, to the iron loss reduction. RPTC suppresses the harmonic currents, which are periodic disturbances, and prevents the increase of iron loss caused by them. Simulation will confirm that the presence or absence of harmonic currents affects the iron loss reduction. Experiments will also show that RPTC reduces the iron loss of IPMSM.

Keywords: IPMSM, iron loss, harmonic current suppression, repetitive perfect tracking control

1. Introduction

PMSM has many advantages such as high output power and controllability, and is widely used in the industrial field. Particularly, interior permanent magnet synchronous motor (IPMSM) is often used for electric vehicles due to its large torque. For further effective utilization of energy, it is necessary to drive PMSMs with high efficiency through control.

Analyzing the causes of driving loss and taking measures are important in order to achieve the high efficient motor driving. The loss of PMSM is mainly classified into the copper loss and the iron loss. The copper loss occurs in the motor windings and the iron loss occurs in the electromagnetic steel sheet. Typical examples of high efficient current control are $i_d = 0$ control and maximum torque per ampere (MTPA) control [1]. These methodologies reduce copper loss. However, these are not necessarily the most efficient control methods because they do not take the iron loss into account. Some methods which determine the dq axis current command so that the sum of copper loss and iron loss is minimized have also been developed [2] [3]. However, the tracking performance to current command often depends on the general current PI controller, and there are few studies which examine the effect of changing the current controller on the efficiency.

IPMSM contains various harmonics components of the motor current [4] and these harmonics deteriorate the tracking performance to the current command. In addition, the tracking error caused by the harmonics current increases the iron loss and reduces the overall driving efficiency. In order to suppress periodic disturbances such as harmonics, RPTC has been proposed in the past. RPTC is a repetitive control based on perfect tracking control (PTC) [5] [6] [7].

In this paper, the effect of suppressing the harmonic currents on the iron loss is verified by comparing the iron loss results of dq axis current control of IPMSM with PI controller only and RPTC. The verification is conducted by simulation and experiment.

2. Iron loss of PMSM

2.1 Causes of iron loss The iron loss occurs in the iron core of PMSM and is broadly classified into the hysteresis loss and the eddy current loss [8]. The IPMSM core contains various harmonic components of magnetic flux density, and these components increase the iron loss caused by minor loops of the hysteresis loop [9] [10].

In the simulation, suppressed and not suppressed motor harmonic currents are set, and the effect of magnitude of harmonics on the iron loss is checked from the magnitude of the hysteresis and eddy current loss.

The experiment will confirm the possibility that the iron loss can be suppressed by the current controller improvement.

2.2 Simulation The change in iron loss caused by the harmonic current presence is verified by simulation. JMAG-Designer (JSOL) is used for the electromagnetic field analysis and the iron loss analysis, and the direct linkage function of JMAG-Designer and MATLAB & Simulink (MathWorks) is used for the simulation of PI current control. The simulation model which has the same stator and rotor dimensions as the IPMSM used in the experiment is shown in Fig. 1. This is a 1/6 partial model for the simulation motor size, and the analysis is performed for 60 degrees. This result is converted to a full model using periodicity to reduce the

* The University of Tokyo
5-1-5, Kashiwanoha, Kashiwa, Chiba, 227-8561 Japan
** DAIKIN INDUSTRIES, Ltd.
1-1-1, Nishi-Hitotsuya, Settsu, Osaka 566-8585, Japan

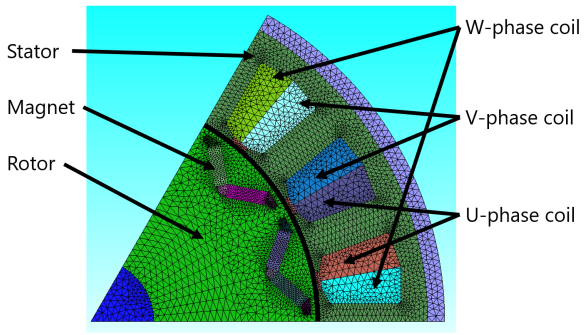

Fig. 1. IPMSM model on simulation (1/6 model (60°)).

Table 1. Parameters of simulation IPMSM.

Parameter	Value
d axis inductance L_d	1.03 mH
q axis inductance L_q	1.31 mH
Resistance R	85 mΩ
Permanent magnet flux linkage K_e	31.2 mWb
Number of pole pairs P	6

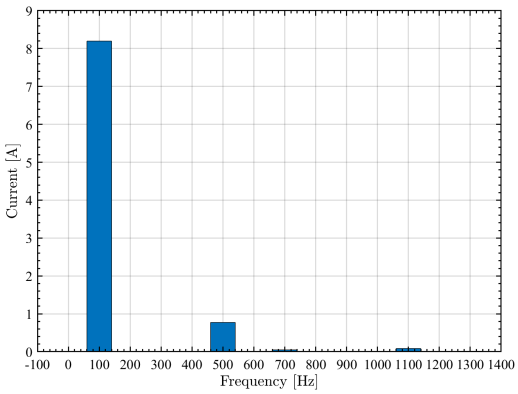

Fig. 2. The amplitude of simulated motor phase current.

Table 2. The result of simulation.

Loss	with harmonics	without harmonics
Hysteresis loss	3.764 W	3.746 W
Eddy current loss	1.289 W	1.271 W
Total iron loss	5.053 W	5.017 W

calculation scale. 35A360 (JSOL) is used for the material of electromagnetic steel sheet, and N39UH (Shin-Etsu Chemical) is used for the material of magnet.

The parameters of this model are listed in Table 1. The values of the residual flux density and coercivity of magnets in the simulation are adjusted so that the permanent magnet flux linkage K_e matches that of the experimental motor.

First, the dq axis current of JMAG motor model is controlled by the PI controller including PWM inverter model of Simulink model. Phase currents and typical order harmonics (n = 5, 7, 11, 13) in steady state are recorded. As simulation conditions, q axis current is set to 10 A and d axis current is set to −0.892 A according to MTPA as follows [11]:

$$i_{d\,ref} = \frac{K_e}{2(L_q - L_d)} - \sqrt{\frac{K_e^2}{4(L_q - L_d)^2} + i_{q\,ref}^2}. \tag{1}$$

The iron loss is simulated using only JMAG. In order to make the simulation time realistic, the inverter model is not considered in the simulation of iron loss, and the phase current values in steady state are used to avoid calculating the loss in transient state.

The rotation speed is set as 1000 rpm. The amplitude of each component of phase currents including harmonics set under this condition is shown in Fig. 2. The trend of iron loss caused by the presence of harmonics is investigated by comparing this motor current and ideal current source.

The results of iron loss with and without harmonics are shown in Table 2. The iron loss values in this table are averaged over one period of the electric angle. From this result, it is confirmed that the removal of harmonic currents reduces the hysteresis loss and the eddy current loss, and the total iron loss is reduced by about 0.71% compared to that when the harmonic currents are included. Therefore, RPTC which suppresses the harmonic currents, is expected to be effective in reducing the iron loss.

3. Overview of RPTC

3.1 Plant model of IPMSM

The IPMSM model on dq coordinate system is shown in Fig. 3. The meaning of each parameter is given in Table 3. In this study, perfect tracking controller and PI controller are designed on dq coordinate. The dq axis voltage equation is expressed as follows:

$$\begin{bmatrix} v_d \\ v_q \end{bmatrix} = \begin{bmatrix} R + sL_d & -\omega_e L_q \\ \omega_e L_d & R + sL_q \end{bmatrix} \begin{bmatrix} i_d \\ i_q \end{bmatrix} + \begin{bmatrix} 0 \\ \omega_e K_e \end{bmatrix}. \tag{2}$$

Since the dq axis current has coupling terms, the decoupling control is widely used. In order to eliminate the coupling terms, the dq voltages are calculated as follows:

$$v_d = v_d' - \omega_e L_q i_q, \tag{3}$$

$$v_q = v_q' + \omega_e (L_d i_d + K_e). \tag{4}$$

State variables are defined as the dq axis current and inputs are defined as the decoupled dq axis voltage. The IPMSM continuous time equation of state is expressed as follows:

$$\dot{\boldsymbol{x}}(t) = A_c \boldsymbol{x}(t) + B_c \boldsymbol{u}(t),\ \boldsymbol{y}(t) = C_c \boldsymbol{x}(t) + D_c \boldsymbol{u}(t), \tag{5}$$

where

$$\boldsymbol{x}(t) = \begin{bmatrix} i_d(t) \\ i_q(t) \end{bmatrix},\ \boldsymbol{u}(t) = \begin{bmatrix} v_d'(t) \\ v_q'(t) \end{bmatrix}, \tag{6}$$

$$\begin{cases} A_c = \begin{bmatrix} -\frac{R}{L_d} & 0 \\ 0 & -\frac{R}{L_q} \end{bmatrix},\ B_c = \begin{bmatrix} \frac{1}{L_d} & 0 \\ 0 & \frac{1}{L_q} \end{bmatrix}, \\ C_c = \begin{bmatrix} 1 & 0 \\ 0 & 1 \end{bmatrix},\ D_c = O. \end{cases} \tag{7}$$

3.2 PTC

The block diagram of PTC on the dq axis is shown in Fig. 4. The subscripts d and q indicate that each coefficient and variable discussed is calculated on that axis. The PTC system has feedforward controller and feedback controller ($C_2[z]$). The feedforward controller is the stable inverse system and achieve zero error to the target value at the sampling points [5]. For n order plant model, it is usually necessary to switch the control input n times. In the case

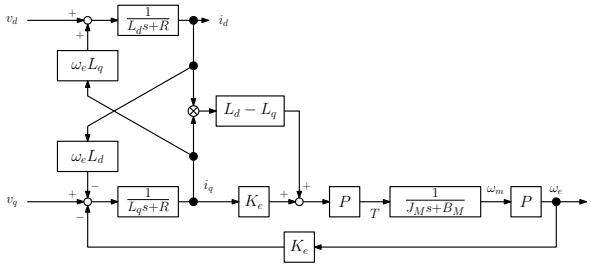

Fig. 3. Block diagram of IPMSM.

Table 3. Parameters of IPMSM and those meanings.

Parameter	Meaning
v_d, v_q	dq axis voltage
i_d, i_q	dq axis current
L_d, L_q	dq axis inductance
R	Resistance
K_e	Permanent magnet flux linkage
P	Number of pole pairs
J_M	Inertia
B_M	Viscous friction coefficient
ω_m	Mechanical angular velocity
ω_e	Electric angular velocity

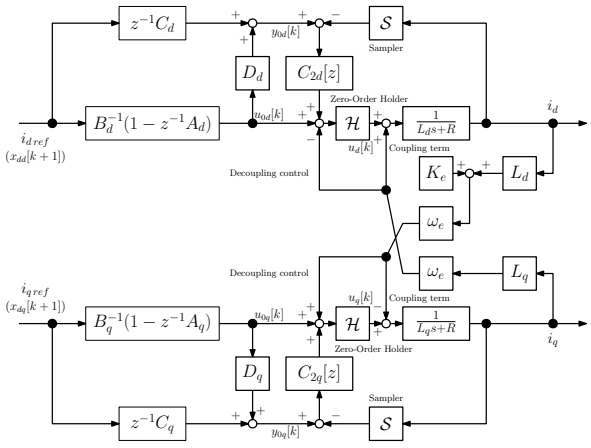

Fig. 4. Block diagram of PTC (dq axis current).

of the IPMSM, the plant is a one-order model and controlled by the single rate controller.

For designing the feedfoward controller, the IPMSM discrete time equation of state is shown in equation (8). This equation is obtained by discretizing equation (5) by the zero order hold (ZOH). The control input period (T_u) is used for discretization. From equation (8), the stable inverse model and nominal output are expressed as equation (9) and (10).

$$x[k+1] = Ax[k] + Bu[k],\ y[k] = Cx[k] + Du[k]. \quad (8)$$

$$u_0[k] = B^{-1}(1 - z^{-1}A)x_d[k+1], \quad (9)$$

$$y_0[k] = z^{-1}Cx_d[k+1] + Du_0[k]. \quad (10)$$

In reality, there are disturbances and modeling errors. However, these are suppressed by a feedback controller $C_2[z]$, and the tracking performance is basically improved by the feedforward controller. $C_2[z]$ is discretized PI controller.

3.3 RPTC The block diagram of RPTC on the dq axis is shown in Fig. 5. The decoupling control and coupling term are the same as in Fig. 4. The RPTC system has periodic signal generator (PSG) by switch 1 and switch 2. By turning on or off two switches, the error compensation like feedforward or feedback is performed [6] [7]. Switch 1 is turned on to record errors in the memory during one period of the periodic disturbance after reaching the steady state. After recording, switch 1 is turned off and switch 2 is turned on to compensate the tracking error caused by the disturbance as a feedforward controller. Feedforward compensation has the advantage of not exacerbating inter harmonics. However, in this experiment, feedback compensation is used due to factors such as modeling errors. For feedback compensation, switch 1 and switch 2 are always ON.

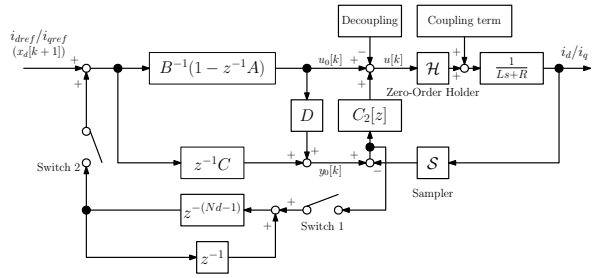

Fig. 5. Block diagram of RPTC (dq axis current).

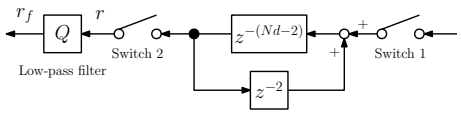

Fig. 6. Block diagram of PSG including low pass filter.

The size of memory is defined as N_d. The memory size N_d is expressed as equation (11) using one tracking error period T_d and control period T_s.

$$N_d = \frac{T_d}{T_s}. \quad (11)$$

For the implementation, a low pass filter with no phase delay is applied to the compensation signal to remove the sensor noise. This low pass filter is expressed as follows:

$$r_f[k] = \frac{z + \gamma + z^{-1}}{\gamma + 2} r[k], \quad (12)$$

where $r_f[k]$ is filter output,$r[k]$ is PSG output and γ is a design parameter of the filter. In this experiment, γ is set to 2, and the cutoff frequency of this filter is 1.8 kHz. The block diagram of the PSG including the low pass filter is shown in Fig. 6.

3.4 Feedback controller design The current PI controller $C_{PI}(s)$ is designed by pole zero cancellation method and expressed as follows:

$$C_{PI}(s) = \frac{Ls + R}{\tau s}. \quad (13)$$

Considering equation (5), the transfer function from the reference current $i_{d,qref}$ to the PMSM dq current $i_{d,q}$ is derived as follows:

$$\frac{i_{d,q}}{i_{d,qref}} = \frac{1}{\tau s + 1}. \quad (14)$$

In this study, T_s is set as 0.1 ms and τ is set as $10T_s = 1$ ms. $C_2[z]$ is obtained from $C_{PI}(s)$ by Tustin Transformation. The period of transform is T_s. RPTC has feedforward controller and $C_2[z]$. The conventional method has only this feedback controller.

4. Experiment

4.1 Experimental setup and condtions The experimental setup is shown in Fig. 7 and the parameters of IPMSM used in this experiment are shown in Table 4. Since this is a single rate control, T_u and T_s are the same value and set to 0.1 ms.

As the drive conditions, the q axis current command is set to $i_{q\,ref} = 10\,\mathrm{A}$ and d axis current command is set to $i_{d\,ref} = -1.86\,\mathrm{A}$ according to the MTPA equation (1) and Table 4. The rotation speed is kept to 1000 rpm by the load servo motor. Thus, the electrical angular frequency is 100 Hz. The fundamental frequency of the tracking error to be suppressed by RPTC is set as the mechanical angular frequency. Thus, the memory size N_d is determined as 600 from the equation (11).

In the loss measurement experiment, the sum of iron loss and mechanical loss is calculated by subtracting the IPMSM output and copper loss from the input power as follows:

$$P_{ir,me} = P_{ir} + P_{me} = P_{in} - P_{out} - P_{co}, \tag{15}$$

where P_{in} is input power, P_{out} is ouput power, P_{co} is copper loss, P_{ir} is iron loss, P_{me} is mechanical loss and $P_{ir,me}$ is the sum of P_{ir} and P_{me}. The power meter measures the input power and phase currents. The copper loss is calculated from the phase currents and winding resistance measured in advance as follows:

$$P_{co} = I_{u\,rms}^2 R_u + I_{v\,rms}^2 R_v + I_{w\,rms}^2 R_w, \tag{16}$$

where $I_{u\,rms}$, $I_{v\,rms}$ and $I_{w\,rms}$ are phase currents. R_u, R_v and R_w are resistance of windings.

The output of IPMSM is calculated from the torque measured by the torque meter and the rotation speed measured by the encoder as follows:

$$P_{out} = T_m \omega_m, \tag{17}$$

where T_m is motor torque.

Power meter is PW3390 (HIOKI) which is able to measure electric power with an accuracy of 0.1 W. Torque meter is TMB307/411 (MAGTROL), and this is capable of measuring up to 10 Nm with an accuracy of ±0.1 %.

Measurements of $P_{ir,me}$ are conducted separately by PI control and RPTC for 5 seconds. These procedures as one set are conducted 12 times. Results of $P_{ir,me}$ are compared on the same set, and the average of 10 sets, excluding maximum and minimum differences of $P_{ir,me}$, are shown as loss reduction results.

Thermocouple thermometers are attached the bearing and windings of IPMSM. Since it is difficult to separate the mechanical loss and the iron loss, the bearing temperature is kept constant in the same set to minimize the variation of mechanical loss. Therefore, it can be considered that the difference of $P_{ir,me}$ is the amount of reduction in iron loss P_{ir}. In addition, more accurate copper loss results are calculated by correcting the winding resistance of each phase as follows [12]:

$$R(T_s) = R(T_{si})\{1 + \alpha(T_s - T_{si})\}, \tag{18}$$

where T_s is the winding temperature, T_{si} is the initial winding temperature and α is the temperature coefficient of copper resistance. The experimental conditions are listed in Table 5.

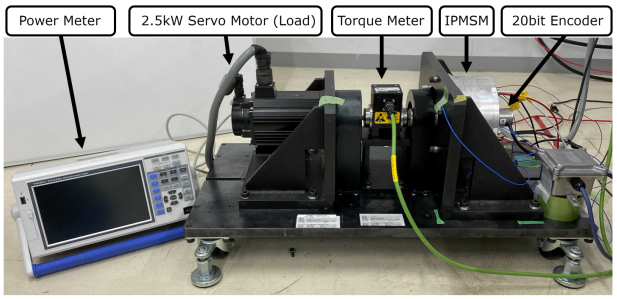

Fig. 7. Experimental setup.

Table 4. Parameters of experimental IPMSM.

Parameter	Value
d axis inductance L_d	0.613 mH
q axis inductance L_q	1.21 mH
Resistance R	85.6 mΩ
Permanent magnet flux linkage K_e	31.2 mWb
Pole pairs P	6
Supply voltage V_{dc}	100 V
Carrier frequency F_s	10 kHz
Control period T_s	0.1 ms
Memory size N_d	600

Table 5. Experimental temperature and phase resistance.

Parameter	Value
Initial winding temperature T_{si}	20.3 °C
U phase resistance $R_u(T_{si})$	86.3 mΩ
V phase resistance $R_v(T_{si})$	88.1 mΩ
W phase resistance $R_w(T_{si})$	86.7 mΩ
Temperature coefficient α	4.30×10^{-3}

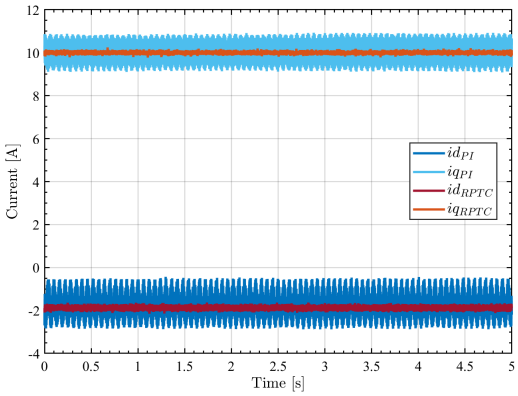

Fig. 8. Dq axis currents of PI and RPTC.

Table 6. Current amplitude of dq axis harmonics (average).

Current amplitude	Fundamental	The 6th harmonic	The 12th harmonic
id_{PI}	1.86 A	632 mA	126 mA
id_{RPTC}	1.86 A	48.2 mA	34.7 mA
iq_{PI}	10.0 A	555 mA	11.7 mA
iq_{RPTC}	10.0 A	33.3 mA	2.14 mA

4.2 Experimental results Fig. 8 shows the dq axis currents of PI control and RPTC. Fig. 9, 10 are FFT results of current control of PI control and RPTC. In addition, Table 6 shows the amplitudes of typical harmonic currents. It is confirmed that RPTC suppresses the 6th and 12th order harmonics significantly.

Table 7 shows the details of power consumption. The values in the table are averages of 10 sets. Assuming that there is

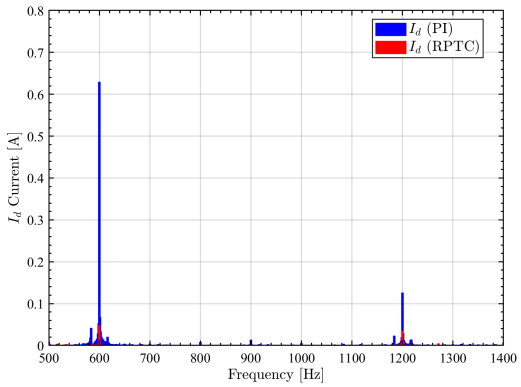

Fig. 9. Comparison of harmonics (d axis current).

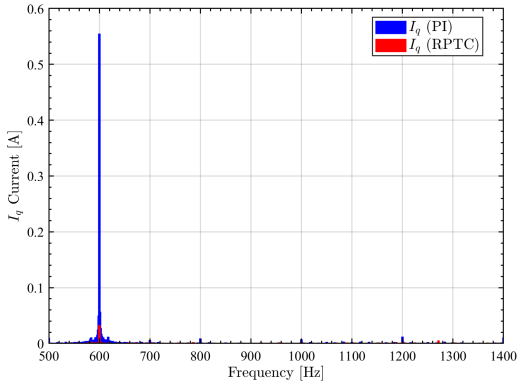

Fig. 10. Comparison of harmonics (q axis current).

Table 7. The details of power consumption (average).

Power consumption	PI	RPTC
Input power P_{in}	298.1 W	299.0 W
Output power P_{out}	272.4 W	274.2 W
Copper loss P_{co}	9.7 W	9.7 W
Iron loss + Mechanical loss $P_{ir,me}$	15.9 W	15.1 W

Table 8. The ratio of loss to input power.

Loss	PI	RPTC
Iron loss + Mechanical loss $P_{ir,me}$	5.4 %	5.1 %
Copper loss P_{co}	3.3 %	3.2 %
Total loss	8.6 %	8.3 %

no variation in the mechanical loss due to the constant bearing temperature, it is confirmed that RPTC reduces the iron loss by 0.8 W under this operating condition. Since the input and output power are different, the ratio of $P_{ir,me}$ and P_{co} to the input power are listed in Table 8 for a fair comparison. Fig. 11 shows these results and error ranges. RPTC reduces the sum of iron loss and mechanical loss from 5.4 % to 5.1 % and the total loss from 8.6 % to 8.3 %.

Due to the accuracy of the measuring instruments, it is not possible to measure the loss with high accuracy. Therefore, the maximum and minimum values of the results are shown in Fig. 11 as the error range. However, the iron loss reduction effect of RPTC is confirmed by repeating the experiment and averaging the results.

In the simulation, it is confirmed that the suppression of harmonic currents reduces the iron loss, and this experiment also shows that suppression of the 6th and 12th order harmonics on the dq axis reduces the IPMSM loss.

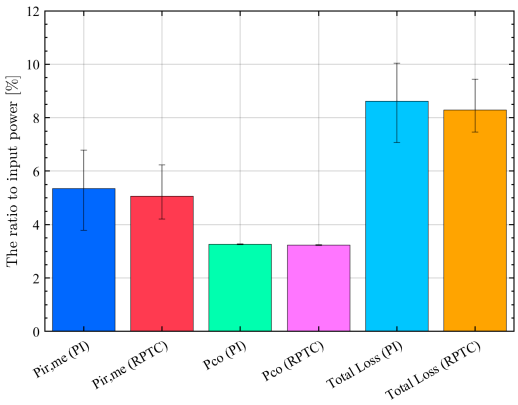

Fig. 11. The ratio of loss and error range.

5. Conclusion

In this paper, the application of RPTC to current control is proposed to reduce the iron loss of IPMSM. It is pointed out that harmonic currents increase the iron loss, and described the method to suppress those harmonics. In RPTC, the harmonic currents of the fundamental frequency are recorded as errors and compensated by the periodic signal generator to suppress harmonics and reduce the iron loss. The simulation results show that the iron loss is reduced when the harmonic currents are eliminated. The experimental results also show that RPTC reduces the iron loss by 0.3 %. In Fig. 11, the variation in output power is large compared to the amount of motor loss. This is due to the large variation of the torque meter relative to the accuracy of power meter and encoder. For the more detailed analysis of the relationship between harmonic currents and iron loss, an appropriate processing method of the torque meter value and a method of separating the iron loss from mechanical loss are required.

There is a research that shows the possibility of improving efficiency when the harmonic current commands are set to other than 0 A [13]. Verification of the change in iron loss and total loss of PMSM when harmonic currents are actively controlled is a future work.

References

(1) T. Inoue, Y. Inoue, S. Morimoto, and M. Sanada, "Maximum Torque per Ampere Control of a Direct Torque-Controlled PMSM in a Stator Flux Linkage Synchronous Frame," *IEEE Transactions on Industry Applications*, vol. 52, no. 3, pp. 2360–2367, 2016.

(2) Q. Guo, C. Zhang, L. Li, J. Zhang, and M. Wang, "Maximum efficiency per torque control of permanent-magnet synchronous machines," *IEEE Transactions on Industrial Electronics*, vol. 62, no. 4, pp. 2135–2143, 2015.

(3) H. Zhang, M. Dou, and J. Deng, "Loss-minimization strategy of nonsinusoidal back EMF PMSM in multiple synchronous reference frames," *IEEE Transactions on Power Electronics*, vol. 35, no. 8, pp. 8335–8346, 2020.

(4) J. Lee, Y. C. Kwon, and S. K. Sul, "Experimental Identification of IPMSM Flux-Linkage Considering Spatial Harmonics for High-Accuracy Simulation of IPMSM Drives," *2018 IEEE Energy Conversion Congress and Exposition, ECCE 2018*, pp. 5804–5809, 2018.

(5) H. Fujimoto, Y. Hori, and A. Kawamura, "Perfect tracking control based on multirate feedforward control with generalized sampling periods," *IEEE Transactions on Industrial Electronics*, vol. 48, no. 3, pp. 636–644, 2001.

(6) T. Nakai and H. Fujimoto, "Harmonic current suppression method of SPM motor based on repetitive perfect tracking control with speed variation," *IECON Proceedings (Industrial Electronics Conference)*, no. 2, pp. 1210–1215, 2008.

(7) H. Fujimoto and T. Takemura, “High-precision control of ball-screw-driven stage based on repetitive control using n-times learning filter,” *IEEE Transactions on Industrial Electronics*, vol. 61, no. 7, pp. 3694–3703, 2014.
(8) K. Yamazaki and A. Abe, “Loss investigation of interior permanent-magnet motors considering carrier harmonics and magnet eddy currents,” *IEEE Transactions on Industry Applications*, vol. 45, no. 2, pp. 659–665, 2009.
(9) H. Nam, K. H. Ha, J. J. Lee, J. P. Hong, and G. H. Kang, “A study on iron loss analysis method considering the harmonics of the flux density waveform using iron loss curves tested on epstein samples,” *IEEE Transactions on Magnetics*, vol. 39, no. 3 I, pp. 1472–1475, 2003.
(10) K. Narita, H. Sano, T. Yamada, R. Akaki, and M. Aoyama, “An Accurate Iron Loss Analysis Method Based on Finite Element Analysis Considering Dynamic Anomalous Loss,” *2018 IEEE Energy Conversion Congress and Exposition, ECCE 2018*, no. ohm m, pp. 4309–4314, 2018.
(11) S. Morimoto, M. Sanada, and Y. Takeda, “Wide-Speed Operation of Interior Permanent Magnet Synchronous Motors with High-Performance Current Regulator,” *IEEE Transactions on Industry Applications*, vol. 30, no. 4, pp. 920–926, 1994.
(12) H. Iwata, K. Ohishi, Y. Yokokura, Y. Okada, Y. Ide, D. Kuraishi, and A. Takahashi, “Robust Estimation Method for Stator Temperature Based on Voltage Disturbance Observer Autotuning Resistance for SPMSM,” *IEEJ Journal of Industry Applications*, vol. 9, no. 4, pp. 341–350, 2020.
(13) K. Yoshimoto and Y. Kitajima, “A Novel Harmonic Current Control for IPMSMs,” *The 2005 International Power Electronics Conference A Multi-Mode Charging Circuit for Rechargeable Batteries*, pp. 1569–1574, 2005.